



Published in final edited form as:

*Pediatr Res.* 2020 December ; 88(6): 925–933. doi:10.1038/s41390-020-0841-6.

## Non-invasive optical measurement of microvascular cerebral hemodynamics and autoregulation in the neonatal ECMO patient

David R. Busch<sup>1</sup>, Wesley B. Baker<sup>2</sup>, Constantine D. Mavroudis<sup>3</sup>, Tiffany S. Ko<sup>4</sup>, Jennifer M. Lynch<sup>5</sup>, Ann L. McCarthy<sup>2</sup>, Genevieve Du Pont-Thibodeau<sup>6</sup>, Erin M. Buckley<sup>7</sup>, Marin Jacobowitz<sup>2</sup>, Timothy Boorady<sup>2</sup>, Kobina Mensah-Brown<sup>2</sup>, James Connelly<sup>8</sup>, Arjun G. Yodh<sup>4</sup>, Todd J. Kilbaugh<sup>9</sup>, Daniel J. Licht<sup>2</sup>

<sup>1</sup>Departments of Anesthesiology & Pain Management and Neurology & Neurotherapeutics, University of Texas Southwestern Medical Center, Dallas, TX

<sup>2</sup>Division of Neurology, Department of Pediatrics, Children's Hospital of Philadelphia, Philadelphia, PA

<sup>3</sup>Division of Cardiovascular Surgery, Department of Surgery, Hospital of the University of Pennsylvania, Philadelphia, PA

<sup>4</sup>Department of Physics and Astronomy, University of Pennsylvania, Philadelphia, PA

<sup>5</sup>Department of Anesthesiology, Hospital of the University of Pennsylvania, Philadelphia, PA

<sup>6</sup>Department of Pediatrics, CHU Sainte-Justine, Montreal, Quebec, Canada

<sup>7</sup>Wallace H. Coulter Department of Biomedical Engineering, Georgia Institute of Technology and Emory University and Department of Pediatrics, School of Medicine, Emory University, Atlanta, GA

<sup>8</sup>ECMO Center, Children's Hospital of Philadelphia, Philadelphia, PA

<sup>9</sup>Department of Anesthesiology and Critical Care Medicine, Children's Hospital of Philadelphia, Philadelphia, PA

### Abstract

Users may view, print, copy, and download text and data-mine the content in such documents, for the purposes of academic research, subject always to the full Conditions of use:[http://www.nature.com/authors/editorial\\_policies/license.html#terms](http://www.nature.com/authors/editorial_policies/license.html#terms)

Corresponding author: Daniel J. Licht, CHOP, 3401 Civic Center Blvd, Philadelphia, PA 19104, LICHT@email.chop.edu, Phone: 267-425-9240, Fax: 215-590-1771.

#### Author contributions

Substantial contributions to conception and design, acquisition of data, or analysis and interpretation of data: DRB, WBB, CDM, TSK, JML, ALM, GDP-T, EMB, MJ, TB, KM-B, AGY, DJL

Drafting the article or revising it critically for important intellectual content: DRB, WBB, JC, CDM, TSK, AGY, TJK, DJL

Final approval of the version to be published: all authors

#### Disclosure statement

DRB, WBB, AGY, DJL have patents and patent applications related to diffuse correlation and optical spectroscopies. These patents have not been licensed and the authors receive no revenue.

#### Category of Study

Clinical Research Article

#### Patient Consent

Under a protocol approved by the Institutional Review Board of the Children's Hospital of Philadelphia, informed consent was obtained by a physician researcher from each subject's parents.

**Background**—Extra-Corporeal Membrane Oxygenation (ECMO) is a life-saving intervention for severe respiratory and cardiac diseases. However, 50% of survivors have abnormal neurologic exams. Current ECMO management is guided by systemic metrics, which may poorly predict cerebral perfusion. Continuous optical monitoring of cerebral hemodynamics during ECMO holds potential to detect risk factors of brain injury such as impaired cerebrovascular autoregulation (*CA*).

**Methods**—We conducted daily measurements of microvascular cerebral blood flow (*CBF*), oxygen saturation, and total hemoglobin concentration using diffuse correlation spectroscopy (DCS) and frequency-domain diffuse optical spectroscopy in 9 neonates. We characterize *CA* utilizing the correlation coefficient (*DCSx*) between *CBF* and mean arterial blood pressure (*MAP*) during ECMO pump flow changes.

**Results**—Average *MAP* and pump flow levels were weakly correlated with *CBF* and were not correlated with cerebral oxygen saturation. *CA* integrity varied between individuals and with time. Systemic measurements of *MAP*, pulse pressure, and left cardiac dysfunction were not predictive of impaired *CA*.

**Conclusions**—Our pilot results suggest that systemic measures alone cannot distinguish impaired *CA* from intact *CA* during ECMO. Furthermore, optical neuromonitoring could help determine patient-specific ECMO pump flows for optimal *CA* integrity, thereby reducing risk of secondary brain injury.

## 1. Introduction

Extra-Corporeal Membrane Oxygenation (ECMO) has been utilized for refractory respiratory and/or cardiac failure in children for over 20 years (1). In this study, we focus on veno-arterial (VA) ECMO, which involves cannulation of large vessels to divert a portion of venous flow through a membrane oxygenator and mechanical pump (2). ECMO provides support to both the heart and lungs by returning oxygenated blood to the body. The long-term neurological morbidity rate for pediatric ECMO survivors is more than 50% (1, 3), prompting increased attention to improving ECMO management of ECMO (1, 4).

Current management of ECMO is guided by age-appropriate mean arterial blood pressure (*MAP*) and blood gas parameters. Accordingly, aberrant changes in *MAP* typically trigger adjustments in pump flow to maintain *MAP* targets and thus end organ perfusion. For the brain, this paradigm assumes *MAP* variations are directly coupled to cerebral blood flow (*CBF*) changes, in effect, assuming cerebrovascular autoregulation (*CA*) is disrupted. Prior work exploring *CA* during pediatric ECMO, however, did not directly monitor *CBF* at the bedside in humans (5–9). While *CBF* monitoring using xenon clearance techniques has been explored (10), this is not practical for continuous bedside monitoring.

To this end, we introduce a non-invasive hybrid optical approach for cerebral monitoring during ECMO. Our instrumentation utilizes diffuse correlation spectroscopy (DCS) to measure *CBF* and frequency-domain diffuse optical spectroscopy (FD-DOS) to measure hemoglobin concentrations and optical scattering. This DOS+DCS approach has been deployed to study other pediatric diagnoses (11, 12), but has not previously been applied to ECMO. DCS provides a quantitative *CBF* index that enables evaluation of the temporal

correlation between *MAP* and *CBF* to assess the integrity of *CA* in individuals and as a function of time. Thus, in this work, we directly measure cerebral hemodynamics to explore the hypothesis that *CA* is impaired during ECMO.

Specifically, we measured the correlation between *CBF* and *MAP* to assess *CA*, and we examined the variability of *CA* within and between individuals during ECMO. We found that this variability is not predicted by systemic measures of *MAP*, pulse pressure, and left cardiac dysfunction. This finding motivates the need for direct, individualized, and continuous assessment of *CA*.

FD-DOS also quantifies cerebral microvascular oxygen saturation (*StO<sub>2</sub>*) and total hemoglobin concentration (*Hb<sub>t</sub>*), which we compared with systemic *MAP* and pump flow levels. Our inter-subject results were highly heterogeneous for *CA* integrity and cerebral hemodynamics, likely in part due to ECMO patient heterogeneity. Ultimately, DOS+DCS metrics have potential to identify temporal periods of high risk for neurological injury, enabling personalized intervention. This pilot study demonstrates the potential of DOS+DCS to provide additional bedside insight into cerebral health.

### 1.1 Cerebrovascular Regulation (Autoregulation) and ECMO Therapy: Background

*CA* mechanisms control cerebrovascular resistance to maintain adequate *CBF* to meet metabolic demands (13, 14). Within the *MAP* limits of pressure autoregulation, these mechanisms guard against the development of inadequate or excessive cerebral blood flow that can produce ischemic or hyperemic brain injury (Figure 1b). Although this view of *CA* has been challenged (13, 15), we adopt Lassen's relatively simple model (16) for the quasi-static flow states in this experiment.

The ECMO circuit provides a source of steady perfusion in parallel with the heart's pulsatile perfusion (Figure 1c); the relative contributions vary between patients and over time. During ECMO, clinicians often adjust *MAP* using pump flow (*PF*), based on systemic vital signs (1). As these metrics lack specificity for brain perfusion, such adjustments may produce blood pressures outside an individual's current autoregulatory range, causing inappropriate cerebral perfusion pressure. This problem is worsened by the disruption of other *CA* mechanisms during ECMO (5, 17–19).

Difficulties also exist with assessing brain health during ECMO. Neonatal neurological exams are compromised by developmental stage and sedation, leading to the use of EEG and cranial ultrasound, but neither can provide high-quality *predictions* or *evaluations* of neuro-injury (1), *e.g.*, ~50% of neonates with 'normal' ultrasounds have abnormal MRI post-ECMO (20). Although a few studies have used oxygen saturation to investigate cerebral perfusion (6–8), there is limited understanding of adequate cerebral perfusion during ECMO (10, 21) or Page 7 of 33 the normative blood pressure range of *CA* (9). DCS and FD-DOS are promising tools to address these needs.

## 1.2 Diffuse Optical and Correlation Spectroscopies

DOS and DCS are related technologies which utilize light ~650–950 nm to probe tissue. While DOS measures chromophore concentrations (primarily oxy- and deoxy-hemoglobin), DCS measures moving scattering bodies (primarily red blood cells).

FD-DOS uses intensity-modulated light to probe the head and brain. A diffusion model of light transport allows separation of the effects of tissue absorption from scattering (22). This separation, combined with multi-wavelength measurements, enables quantitative estimates of oxy- and deoxy-hemoglobin concentrations, and thus of  $StO_2$  and  $Hb_t$ . By contrast, devices utilizing constant or slowly-varying light sources (*e.g.*, many commercial cerebral oximeters (23, 24)) are unable to separate scattering from absorption and are therefore limited to trend monitoring. Quantitative optical measurements are important during changing physiological conditions, *e.g.*, developing edema during ECMO.

In addition to FD-DOS, DCS employs photon correlation techniques to derive a blood flow index (*BFI*) proportional to *CBF* (25–27). Combining these devices into a hybrid system allows simultaneous measurement of blood flow, hemoglobin content, and hemoglobin oxygen saturation. A major advantage of DOS+DCS is the ability to make serial or continuous measurements. In part, our study sought to identify temporal changes in cerebral hemodynamics during ECMO.

## 2. Methods

All patients from English-speaking families cannulated for VA-ECMO at the Children's Hospital of Philadelphia were eligible for enrollment. The responsible clinical team was consulted prior to approach for enrollment and each measurement. Clinically unstable subjects were excluded from the study. Under an Institutional Review Board approved protocol, informed consent was obtained by a physician researcher. Several metrics of overall and cardiac health were calculated for each study participant. A Functional Status Score (28) was calculated at both ICU admission and discharge; Pediatric Risk of Mortality III Scores (29) were also calculated. Arterial pulse pressure ( $PP = \text{systolic} - \text{diastolic BP}$ ) was examined as a readily available metric of cardiac health. Clinically-ordered echocardiograms were assessed for cardiac dysfunction.

Upon enrollment, ~1-hour daily optical FD-DOS/DCS monitoring sessions were conducted (Table 1). Monitoring ended due to clinical instability, weaning from or withdrawal of ECMO, parental choice, or at the 5<sup>th</sup> day of ECMO. The monitoring session consisted of two phases: (1) baseline measurements of *BFI*,  $StO_2$ , and  $Hb_t$  and (2) *CA* assessment. Subject measurements with low-quality signal (*e.g.*, DCS photon count rate < 10 kHz), non-neonates, and recipients of extended (>15 min) CPR were excluded from the current analysis. Additionally, measurements following dramatic swelling in one subject (>30% change in bodyweight) were excluded due to potential failure of the diffusion approximation. Study personnel continuously observed the subjects during data collection. Motion artifacts were manually recorded and these periods excluded from further analysis. Additionally, artifacts were identified using both the temporal derivative and absolute value of blood pressure and pump flow.

## 2.1 Baseline Measurements and CA Assessment

Details of the hybrid DOS+DCS instrument have been described elsewhere and are summarized in the online supplement (30). A semi-infinite model was used for analysis of both DOS and DCS data. Baseline measurements were collected each day using a custom-built flexible patient interface with embedded fiber optics manually placed on the subject's forehead. Measurements were limited to the right side only due to cannula placement. For each baseline period of ~5 min., tissue oxygen saturation ( $StO_{2o}$ ), hemoglobin content ( $Hb_{to}$ ), and reduced scattering coefficient ( $\mu'_{so}$ ) were quantified.

After the baseline measurements, a lighter and more conformable DOS+DCS probe was utilized for CA measurements. FD-DOS measurements of  $StO_2$  and  $Hb_t$  utilized a single source-detector separation to calculate temporal changes from baseline (31). FD-DOS temporal data was only available for 15 of 22 monitoring sessions. The DOS measurement was sensitive to signal-to-noise issues due to the relatively small source and detector fibers required for the lightweight probe.

For the CA assessment phase, interleaved FD-DOS and DCS measurements were acquired every 7 seconds on the subject's right forehead during serial PF variation (Figure 1a, 30–60 minutes, depending on toleration of flow variation). In addition to the optical data, time-synchronized clinical vital signs, and ECMO system parameters (Transonic HT-100 flow meter, Spectrum Medical M2) were recorded (CNS, Moberg Research). These data included pulse and mean arterial pressures ( $PP$ ,  $MAP$ ), venous oxygen saturation ( $SvO_2$ ), arterial oxygen saturation ( $SaO_2$ ), and  $PF$  (normalized by weight). Temporal data sets utilized for CA assessment were normalized to a ~5 min. period prior to any manipulation.

PF changes were performed by the bedside perfusionist in steps of approximately  $\pm 10\%$  from baseline. Each step was maintained for ~5 minutes (Figure 1a) prior to return to baseline PF. In initial measurements (subjects 1, 2), we aimed to undertake four 10% steps (*i.e.*, 80% to 120% of baseline). However, we found patient-specific flow limitations (*e.g.* high venous line pressures) often prevented PF adjustments by the full range. In these cases, a subset of the range was used. As  $\pm 10\%$  changes were found to sufficiently alter  $MAP$ , PF adjustments were subsequently limited to ~90% and ~110% of baseline. The speed and exact timing of the adjustments was left to the perfusionist's discretion, which was guided by the actual and expected response of the patient to flow changes. Note that reported PF is normalized by body weight (L/min/kg).

## 2.2 Data Processing and Statistical Analysis

Baseline cerebral hemodynamic and baseline circulatory parameters (symbolized by  $X_o$ ) were compared across individuals and measurement days. Specifically, we computed the Pearson correlation coefficient between: (1)  $BFI_o$  and  $MAP_o$ ; (2)  $BFI_o$  and  $PF_o$ ; (3)  $PF_o$  and  $MAP_o$ ; (4)  $StO_{2o}$  and  $MAP_o$ ; (5)  $StO_{2o}$  and  $PF_o$ ; (6)  $StO_{2o}$  and  $SvO_{2o}$ ; and (7)  $PP_o$  and  $MAP_o$  (corrcoef, MATLAB R2017a, Mathworks).

For each CA assessment (N=22 Table 1), relative  $MAP$  and  $BFI$  data were computed as a function of monitoring time,  $t$ , during cyclical PF variation (Figure 1a), *i.e.*,  $rMAP(t) \equiv MAP(t)/MAP_o$ ,  $rBFI(t) \equiv BFI(t)/BFI_o$ . CA was characterized by the  $DCSx$  index, which is

the Pearson's correlation coefficient between  $rMAP(t)$  and  $rBFI(t)$ . To examine the impact of baseline circulatory parameters on  $CA$ , we grouped  $DCSx$  measurements by  $MAP_o$  terciles, low/moderate/high  $PP_o$ , and severe/moderate/mild left cardiac dysfunction. A Wilcoxon rank sum test was then employed to test for differences in  $DCSx$  across the three groups for each circulatory parameter. Low/moderate/high  $PP_o$  corresponded to  $PP_o < 8$  mmHg,  $8 < PP_o < 15$  mmHg, and  $PP_o > 15$  mmHg, respectively. Severe/moderate/mild left cardiac dysfunction was assessed by a blinded independent reviewer of clinical echo cardiograms. The reviewer's scores were compared with the clinical assessment scores; the more conservative score was used if there was disagreement. Finally, we present two case examples of concurrent time-series  $rBFI$  and  $StO_2$  data.

### 3. Results

We measured a total of 15 children. The present analysis focuses on neonates. One subject was therefore excluded from the present analysis due to age (7 yr.). Additionally, one subject was excluded due to low DCS signal to noise ratio, and four subjects were excluded due to persistent artifacts in vital signs or  $PF$ . Lastly, one subject was only partially included in this analysis due to significant swelling that occurred between measurement days 1 and 2 (with accompanying body weight change of 2.9 to 3.83kg); this degree of swelling will very likely cause a breakdown of underlying mathematical assumptions in our analysis. All monitoring sessions for the remaining eight neonates were included. Thus, we analyzed 22 monitoring sessions of the nine included neonates (Table 1 supplementary material Figure S1). At our institution, centrifugal pumps are not used for infants, therefore all included subjects were perfused with roller pumps.

#### 3.1 Baseline hemodynamics and vital signs

Table 2 contains summary statistics of baseline hemodynamic measurements across the 9 neonatal subjects (1–5 measurements per subject). Figure 2 shows their correlation with systemic measures. We observed high intrasubject variability in  $BFI_o$ , compared to  $PF_o$  and  $MAP_o$ , which suggests that these systemic parameters are poor surrogates of  $CBF$  (Table 2). Weak correlations between  $BFI_o$  and  $PF_o$  ( $R = -0.45$ ,  $p = 0.03$ ) and between  $BFI_o$  and  $MAP_o$  ( $R = 0.49$ ,  $p = 0.02$ ), were found. Note also that we did not observe a significant correlation between  $MAP_o$  and  $PF_o$  ( $R = -0.24$ ,  $p = 0.28$ ) in this population. These weak and potentially spurious correlations are perhaps further testament to the complex interactions that can exist between ECMO and cardiac circuits and these circuits and the brain, as well as the significant inter-subject and temporal variation in vasopressor therapy, shock state, etc. The intra-subject variability in  $BFI_o$  could reflect variability within individual patients, e.g., due to changes in superficial tissue thickness. Similarly,  $StO_{2o}$  was not correlated with  $PF_o$  ( $R = 0.11$ ,  $p = 0.64$ ) or with  $MAP_o$  ( $R = 0.07$ ,  $p = 0.77$ ), and it was only marginally correlated with mixed systemic  $SvO_{2o}$  ( $R = 0.43$ ,  $p = 0.057$ ). Cerebral  $StO_{2o}$  was generally lower than systemic  $SvO_{2o}$ , which is consistent with the high metabolism of the brain, compared to the resting body, and other work (32), as well as the differences between cerebral and somatic vascular physiology. Finally, the correlations of  $BFI_o$  and  $StO_{2o}$  with  $PP_o$  were  $R = 0.328$  ( $p = 0.136$ ) and  $R = -0.08$  ( $p = 0.745$ ) respectively (not shown).

An important advantage of the FD-DOS technique is its ability to measure *absolute* optical properties. In the 7 neonates with multiple measurement days, we observed an intra-subject temporal coefficient of variation (CV) in the tissue reduced scattering coefficient of 0.26 (0.18, 0.35) (*i.e.*, CV is the ratio of the standard deviation and the mean of  $\mu'_{s,o}$  at 785nm for each patient across multiple monitoring days; inter-subject median (IQR); also see Table 2). Since  $\mu'_{s,o}$  determines the optical path length in tissue, accurate values of  $\mu'_{s,o}$  are critical for quantification. By contrast, tissue absorption ( $\mu_a$ ) varied less (0.09 (0.04, 0.22)).

Functional systems scores and pediatric risk of mortality (III) scores, day of life, and day on ECMO were all compared to optical measurements, and no significant relationships were identified.

### 3.2 CA assessment during ECMO pump flow variation

Figure 3 shows exemplar temporal traces of  $Hb_t$ ,  $StO_2$ , relative  $BFI$ , and relative  $MAP$  measurements obtained during  $\pm 20\%$   $PF$  changes in different neonates (#1, 2) on the first day of ECMO and of life. In these examples,  $Hb_t$  and  $StO_2$  are insensitive to flow manipulations in both cases, while  $MAP$  and  $BFI$  data show divergent responses. These results suggest that baseline condition for subject 2 was hyperoxygenated, as hemoglobin saturation was consistent despite  $>10\%$  decrease in blood flow. For subject 1, the  $DCSx$  index (95% CI) was  $-0.42$  ( $-0.52, -0.31$ ); generally,  $DCSx$  near zero or slightly negative are considered to reflect intact  $CA$ . For subject 2, the  $DCSx$  index of  $0.71$  ( $0.65, 0.77$ ) suggests impaired  $CA$  (Pearson's correlation coefficients between  $StO_2$  and  $MAP$  were  $-0.04$  ( $-0.17, 0.09$ ) and  $0.21$  ( $0.1, 0.32$ ), respectively).

Across the subject population, we found that  $DCSx$  was not predicted by  $MAP_o$ ,  $PP_o$ , or left cardiac dysfunction (Figure 4). While not statistically significant,  $DCSx$  was lower in patients with better cardiac function measured by echo-cardiogram, suggesting  $CA$  is more robust in patients with healthier hearts.

### 3.3 Temporal variation in CA during ECMO

Temporal variation in  $CA$  during ECMO for individual subjects was substantial (*i.e.*, a coefficient of variation of  $0.86$  ( $-0.32, 1.14$ ); see Table 2), and larger than the temporal variation in systemic parameters (Table 2). We Page 13 of 33 further present one longitudinal case example (Figure 5) for the patient with the largest number of monitoring days (subject 7). The robustly positive  $DCSx$  measurements on days 1–3 suggest impaired  $CA$ . In addition,  $MAP_o$ ,  $PP_o$ ,  $PF_o$ , and  $StO_{2o}$  all significantly increased during days 1–3. It is plausible that the increase in  $StO_{2o}$  reflects increased oxygen delivery to the brain arising from excessive blood flow due to the increase in  $MAP_o$ . Conversely, on days 4 and 5,  $DCSx$  is noticeably closer to zero, signaling improved  $CA$ . Further, systemic arterial and venous saturations ( $SaO_{2o}$  and  $SvO_{2o}$ ), between days 1–3 and 4–5 are not significantly different. Finally, the improved  $CA$  on days 4 and 5 was associated with higher  $PP_o$ , a surrogate metric of improved cardiac function. The notion of improved cardiac function is also supported by the divergence between  $PP_o$  and  $PF_o$  on day 4, which suggests that the healing heart is taking over the work of providing perfusion. This patient was successfully weaned from ECMO. Examining all the measurements in the entire population, we do not see a significant

trend in  $DCSx$  with time (not shown). The longitudinal results shown in Figure 5 should be interpreted with caution, in part because the optical measurements were temporally sparse (1 per day) and limited number of total measurements.

## 4. Discussion

In this observational pilot study we introduced and demonstrated a scheme that utilizes diffuse optical technology to non-invasively assess  $CA$  (*i.e.*,  $DCSx$  index), microvascular cerebral perfusion (*i.e.*,  $BFI$ ), and microvascular cerebral oxygenation (*i.e.*,  $StO_2$ ) in neonates receiving ECMO. The optical measurements, which were performed at the bedside with minimal disruption to clinical care of the patient, varied substantially between individuals and with time (Table 2). These preliminary results, as well as previous work by our group (11, 30) and others (33), suggest these optical measurements may be well-suited for longitudinal monitoring in children. Future work is clearly needed to demonstrate the clinical utility of this scheme and the practicality of continuous monitoring in critically ill children.

For  $CA$  assessment, optical measurements of  $BFI$  changes were compared to corresponding  $MAP$  changes induced by  $PF$  manipulations (Figure 3). Pilot data from the case examples demonstrates the scheme's ability to track longitudinal improvement (Figure 5) in an individual neonate during ECMO. By contrast, cardiac and circulatory parameters do not predict  $CA$ , *i.e.*, intact or impaired as defined by  $DCSx$  measurements (Figure 4, Figure 5). Note, previous work has shown good agreement between DCS and Laser Doppler  $CBF$  measures (25) and that  $LDx$  could accurately distinguish intact from impaired  $CA$  (34). This in turn suggests that the  $DCSx$  is comparable to  $LDx$ , measured invasively by Laser Doppler, for determination of  $CA$ .

At clinically prescribed  $PF_o$ , the  $BFI_o$ ,  $MAP_o$ , and  $StO_{2,o}$  levels were heterogeneous (Figure 2); intrasubject variability in  $BFI_o$  and  $CA$  were large compared to the variability of  $PF_o$  and  $MAP_o$  (Table 2). The impact of  $PF_o$  on  $MAP_o$  and ultimately, on cerebral blood flow, appears to be complex; among other factors, it depends on cardiac output and the fraction of necessary flow provided by the ECMO pump, and may also reflect brain injury acquired prior to ECMO initiation. In total, these results suggest that the easily measured systemic parameters, such as pump flow and mean arterial pressure, that are often used to characterize patient response are not always good surrogates for healthy *cerebral physiology* (*i.e.*, adequate  $CBF$  or  $StO_2$ ). Future work is needed to confirm the prognostic value of longitudinal monitoring with this scheme.

### 4.1 Direct Cerebral Monitoring versus Systemic Surrogates

Current clinical protocols frequently rely on systemic variables such as  $MAP$  targets, urine output and skin temperature as surrogates of end-organ perfusion, including cerebral perfusion. This study demonstrates that these non-neurologic indicators of adequate oxygen delivery are not reliable surrogates of brain perfusion (35, 36). We observed longitudinal changes in perfusion and  $CA$  that were not apparent from the systemic measurements (*e.g.*, Figure 5). These pilot results, in combination with the observed variability between absolute  $MAP$ ,  $SaO_{2,o}$ , and  $SvO_{2,o}$  and optical measurements of the brain (Figure 5), highlight the

potential of diffuse optics for improving patient-specific *CBF* management during ECMO. Defining such *CBF* targets will clearly be a challenge, as has been reviewed in the context of neurosurgery (37), and will ultimately need to include both blood pressure and metabolic regulation. Note, quantitative cerebral *StO<sub>2</sub>* measurements were generally lower than systemic *SvO<sub>2</sub>* measurements (Figure 2), which is indicative of higher cerebral oxygen extraction levels (32), as well as differences in vascular physiology. Indeed, our average measured *StO<sub>2</sub>* across patients was 57%, which is lower than previously reported *StO<sub>2</sub>* of 67% in 1-week old healthy infants (33).

Intriguingly, in this population *BFI<sub>0</sub>* was a factor  $\sim 2$  lower, while *StO<sub>2</sub>* was 8% higher, than previously reported pre-surgical values in ventilated neonates with congenital heart defects (27).

#### 4.2 Use of *StO<sub>2</sub>* Data to Assess *CA*

Our preliminary findings indicate that using *StO<sub>2</sub>* measurements alone to assess *CA* may be difficult to generalize. For example, the *StO<sub>2</sub>* data does not distinguish between the 2 case examples presented in Figure 3, while the *BFI* data suggests different states of *CA*. The origin of the differing trends between *BFI* and *StO<sub>2</sub>* data in Figure 3 is not known. From Fick's model, a constant *StO<sub>2</sub>* in the face of changing *BFI* suggests that cerebral oxygen metabolism changes with pump/heart-driven cerebral blood flow, which seems unlikely. Potentially, the high absolute *StO<sub>2</sub>* levels in these two examples (*i.e.*, 60–70%) reflect hyperperfusion, and the accumulation of a sizeable reservoir of dissolved oxygen in the tissue. Previous modeling work has shown that such conditions can substantially blunt the changes in oxygen extraction arising from changes in cerebral blood flow (38).

Excessive *CBF* however, may expose the brain to risk of bleeding. More work is needed to investigate the use of *StO<sub>2</sub>* data for *CA* assessment in this population.

#### 4.3 Intrasubject Variability in Optical Tissue Scattering

Intrasubject temporal variability in the tissue reduced scattering coefficient measurements was  $\sim 30\%$ . Similar variability in scattering was also recently reported in 2 neonates on ECMO (39). The variability in scattering could reflect variability in tissue water content caused by swelling/inflammation. Indeed, given one subject's  $>30\%$  increase in body weight relative to the prior day, the very low tissue scattering coefficient measurement ( $\sim 1.5 \text{ cm}^{-1}$  at 785 nm) on the second day likely indicated a large amount of brain/superficial tissue swelling. Subsequent monitoring sessions were excluded from our analysis, due to potential failure of the diffusion model of photon transport. Additionally, the swelling observed in the ECMO population pushes the skin and optical probe further from the brain. Independent measurements of tissue water content and swelling in future studies is needed to better understand the relationship between scattering and swelling.

Clinical NIRS monitors assume a value for tissue scattering to derive estimates of oxygen saturation (22); errors in this estimation affect the accuracy of computed *StO<sub>2</sub>*. The large temporal variability in scattering observed here raises concern about conflation between scattering and oxygenation changes in NIRS monitoring during ECMO. Future investigation of the magnitude and distribution of this error are needed. In addition, since accurate

calculation of the DCS  $BFI$  relies on accurate knowledge of tissue absorption and scattering (22), a hybrid frequency or time domain DOS+DCS approach is preferable to DCS alone for perfusion monitoring.

#### 4.4 Limitations

This pilot study has many limitations. The patient population is heterogeneous, even within diagnosis. Post-ECMO neuroimaging showed a wide range of injury; our sample size and the limitations discussed below preclude drawing conclusions on the relationship between  $CA$  and the injury observed weeks after ECMO by MRI. In addition, the study had variation in the timing of ECMO initiation, severity of illness, total blood volume (volume status), and other clinical variables in these critically ill children. Moreover, since the present study is observational, we did not control for medications nor clinical interventions; additionally, our Page 17 of 33 recruitment protocol may have excluded the most ill, least stable, children. Given limited resources, continuous 24-hour monitoring was not practical. Instead, our measurements were acquired over  $\sim 1$  hour per day, scheduled as convenient for the family and clinical team, and thus each measurement had a large variation in measurement time with respect to the start of ECMO, etc. Therefore, the longitudinal data from a single subject presented in Figure 5 should be interpreted with caution, *e.g.*, since the  $\sim 1$ -hour monitoring intervals may not be indicative of average hemodynamics across the day. Further, the precise reasons for the observed improvement in  $CA$  in Figure 5 are not known. Our data was also collected at a relatively slow rate ( $\sim 7$ s per measurement), limiting our sensitivity to higher frequency autoregulatory mechanisms. Due to the small data set, we made a linear comparison of  $MAP$  to  $BFI_o$ , rather than a more realistic piece-wise linear or sigmoidal curve.

Furthermore, in these experiments, data was collected only on the right side of the head. Children were cannulated via the great vessels in the right side of the neck, the left side of the head was therefore positioned towards the bed. Anchoring our probe to the left side of the head in this position was impractical and repositioning was not feasible due to danger of dislodging the cannulas. However, cannulation via the vessels on the right side of the neck may restrict blood flow more to the right than left side of the brain, as the right side is then perfused by collateral circulation through the circle of Willis, leaving the right side of the brain more vulnerable to ischemic injury. Future studies to identify potential hemispherical differences in  $Hb_t$ ,  $StO_2$ , and  $CA$  are needed.

For the baseline measurements, we caution that the variability in  $BFI_o$  also likely reflects variability in factors such as differences in the superficial tissue thickness and probe pressure against the head. Swelling, for example, may change the distance between the optical probe and the brain, which will affect the absolute  $BFI$  measurement. Note, however, the relative changes used for the  $CA$  measurements are more robust to many of these effects.

## 5. Conclusion

We carried out a pilot study that employed diffuse optical tools to continuously monitor cerebral hemodynamics and assess cerebrovascular autoregulation integrity in the intensive care unit during VA-ECMO. Given a lack of correlation between DCS-measured  $CBF$  and

both *PF* and *MAP*, the data here present a strong argument for cerebral monitoring with individualization of end-organ targeted care. This argument is further reinforced by the substantial variability in measurements of cerebral hemodynamics and *CA* integrity across patients and with time. This variability was not predicted by systemic measurements. Cerebral monitoring with diffuse optics could, in principal, be used to drive ECMO care and improve the quality of survival in these critically ill neonates. The hybrid FD-DOS+DCS approach utilized in this study provided additional value compared to FD-DOS alone for assessment of *CA*, oxygen delivery, and metabolism. Looking forward, by determining these critical metrics of cerebral health, quantitative optical tools could permit goal-directed clinical interventions, *e.g.*, setting of ECMO pump flow based on *DCS<sub>x</sub>* values.

## Supplementary Material

Refer to Web version on PubMed Central for supplementary material.

## Acknowledgements

The authors thank the study participants and their families. We also thank Dr. Ashwin Parthasarathy, Dr. Turgut Durduran, Dr. Robert Sutton, Dr. Robert Levy, and Dr. Jeffery Cochran, for helpful discussions; Dr. Brian White for clinical insights; Kenneth Abramson for technical assistance; and the CHOP ECMO team, Madeline Winters, John Newland, and Kaitlin Griffith, for assistance in making measurements.

Financial support

National Institutes of Health (NIH R01-NS072338, T32-HL007915, R01-NS060653, F31-HD085731, R01-HL141386, & P41-EB015893), DoD CDMRP W81XWH1810607, the Thrasher Foundation, Institute of International Education, and philanthropic support from the June and Steve Wolfson Family Foundation and the Raymond Family ECMO Fund.

## References

1. Lin N, Flibotte J, Licht DJ 2018 Neuromonitoring in the neonatal ECMO patient *Semin Perinatol*. Elsevier.
2. Lequier L 2004 Extracorporeal life support in pediatric and neonatal critical care: a review. *J Intensive Care Med* 19:243–258. [PubMed: 15358943]
3. Ijsselstijn H, van Heijst AF 2014 Long-term outcome of children treated with neonatal extracorporeal membrane oxygenation: increasing problems with increasing age. *Semin Perinatol* 38:114–121. [PubMed: 24580767]
4. Bembea MM, et al. 2015 Neuromonitoring during extracorporeal membrane oxygenation: a systematic review of the literature. *Pediatr Crit Care Med* 16:558–564. [PubMed: 25828783]
5. Lee JK, et al. 2014 A pilot study of cerebrovascular reactivity autoregulation after pediatric cardiac arrest. *Resuscitation* 85:1387–1393. [PubMed: 25046743]
6. Papademetriou M, et al. 2013 Wavelet Cross-Correlation to Investigate Regional Variations in Cerebral Oxygenation in Infants Supported on Extracorporeal Membrane Oxygenation. *Oxygen Transport to Tissue XXXIV* 765:203–209.
7. Van Heijst A, et al. 2004 Oxygenation and hemodynamics in left and right cerebral hemispheres during induction of veno-arterial extracorporeal membrane oxygenation. *The Journal of pediatrics* 144:223. [PubMed: 14760266]
8. Tian F, et al. 2017 Impairment of cerebral autoregulation in pediatric extracorporeal membrane oxygenation associated with neuroimaging abnormalities. *Neurophot*. 4:041410.
9. Zweifel C, Dias C, Smielewski P, Czosnyka M 2014 Continuous time-domain monitoring of cerebral autoregulation in neurocritical care. *Med Eng Phys* 36:638–645. [PubMed: 24703503]

10. Stockwell JA, et al. 1996 Cerebral blood flow and carbon dioxide reactivity in neonates during venoarterial extracorporeal life support. *Crit Care Med* 24:155–162. [PubMed: 8565521]
11. Lynch JM, et al. 2018 Preoperative cerebral hemodynamics from birth to surgery in neonates with critical congenital heart disease. *J Thorac Cardiovasc Surg* 156:1657–1664. [PubMed: 29859676]
12. Diop M, et al. 2015 Development of a combined broadband near-infrared and diffusion correlation system for monitoring cerebral blood flow and oxidative metabolism in preterm infants. *Biomed Opt Express* 6:3907–3918. [PubMed: 26504641]
13. Willie CK, Tzeng YC, Fisher JA, Ainslie PN 2014 Integrative regulation of human brain blood flow. *J Physiol* 592:841–859. [PubMed: 24396059]
14. Czosnyka M, et al. 2009 Monitoring of cerebrovascular autoregulation: facts, myths, and missing links. *Neurocrit Care* 10:373–386. [PubMed: 19127448]
15. Tzeng YC, Ainslie PN 2014 Blood pressure regulation IX: cerebral autoregulation under blood pressure challenges. *Eur J Appl Physiol* 114:545–559. [PubMed: 23737006]
16. Lassen NA 1959 Cerebral blood flow and oxygen consumption in man. *Physiol Rev* 39:183–238. [PubMed: 13645234]
17. Short BL, Walker LK, Bender KS, Traystman RJ 1993 Impairment of cerebral autoregulation during extracorporeal membrane oxygenation in newborn lambs. *Pediatr Res* 33:289–294. [PubMed: 8460067]
18. Papademetriou MD, et al. 2012 Optical topography to measure variations in regional cerebral oxygenation in an infant supported on veno-arterial extra-corporeal membrane oxygenation Oxygen Transport to Tissue XXXIII. Springer, pp 71–76.
19. Short BL 2005 The effect of extracorporeal life support on the brain: a focus on ECMO. *Semin Perinatol* 29:45–50. [PubMed: 15921152]
20. Rollins MD, et al. 2012 Utility of neuroradiographic imaging in predicting outcomes after neonatal extracorporeal membrane oxygenation. *J Pediatr Surg* 47:76–80. [PubMed: 22244396]
21. Taccone FS, et al. 2013 Cerebral oximetry during extracorporeal cardiopulmonary resuscitation. *Crit Care* 17:409. [PubMed: 23356515]
22. Durduran T, Choe R, Baker WB, Yodh AG 2010 Diffuse Optics for Tissue Monitoring and Tomography. *Rep Prog Phys* 73:076701. [PubMed: 26120204]
23. Jenny C, et al. 2011 Reproducibility of cerebral tissue oxygen saturation measurements by near-infrared spectroscopy in newborn infants. *J Biomed Opt* 16:097004–097004. [PubMed: 21950939]
24. Schneider A, et al. 2014 Comparison of 4 near-infrared spectroscopy devices show that they are only suitable for monitoring cerebral oxygenation trends in preterm infants. *Acta Paediatr*.
25. Mesquita RC, et al. 2011 Direct measurement of tissue blood flow and metabolism with diffuse optics. *Philosophical Transactions of the Royal Society a-Mathematical Physical and Engineering Sciences* 369:4390–4406.
26. Boas DA, Yodh AG 1997 Spatially varying dynamical properties of turbid media probed with diffusing temporal light correlation. *Journal of the Optical Society of America A-Optics Image Science and Vision* 14:192–215.
27. Jain V, et al. 2014 Cerebral oxygen metabolism in neonates with congenital heart disease quantified by MRI and Optics. *JCBFM* 34:380–388.
28. Pollack MM, et al. 2009 Functional Status Scale: new pediatric outcome measure. *Pediatrics* 124:e18–28. [PubMed: 19564265]
29. Wang JN, Wu JM, Chen YJ 2001 Validity of the updated pediatric risk of mortality score (PRISM III) in predicting the probability of mortality in a pediatric intensive care unit. *Acta Paediatr Taiwan* 42:333–337. [PubMed: 11811220]
30. Buckley EM, et al. 2013 Early postoperative changes in cerebral oxygen metabolism following neonatal cardiac surgery: Effects of surgical duration. *J Thorac Cardiovasc Surg* 145:196–205. [PubMed: 23111021]
31. Fantini S, et al. 1999 Non-invasive optical monitoring of the newborn piglet brain using continuous-wave and frequency-domain spectroscopy. *Phys Med Biol* 44:1543. [PubMed: 10498522]

32. Lynch JM, et al. 2014 Validation of optically measured cerebral venous oxygenation saturation in humans. *Acad Radiol* 21:162–167. [PubMed: 24439329]
33. Franceschini MA, et al. 2007 Assessment of infant brain development with frequency-domain near-infrared spectroscopy. *Pediatr Res* 61:546–551. [PubMed: 17413855]
34. Brady KM, et al. 2007 Continuous time-domain analysis of cerebrovascular autoregulation using near-infrared spectroscopy. *Stroke* 38:2818–2825. [PubMed: 17761921]
35. Kato R, Pinsky MR 2015 Personalizing blood pressure management in septic shock. *Ann Intensive Care* 5:41. [PubMed: 26573630]
36. Rhee CJ, et al. 2016 Elevated Diastolic Closing Margin Is Associated with Intraventricular Hemorrhage in Premature Infants. *J Pediatr*.
37. Steiner LA, Czosnyka M 2002 Should we measure cerebral blood flow in head-injured patients? *Br J Neurosurg* 16:429–439. [PubMed: 12498485]
38. Valabregue R, et al. 2003 Relation between cerebral blood flow and metabolism explained by a model of oxygen exchange. *J Cereb Blood Flow Metab* 23:536–545. [PubMed: 12771568]
39. Tian F, et al. 2017 Regional Cerebral Abnormalities Measured by Frequency-Domain Near-Infrared Spectroscopy in Pediatric Patients During Extracorporeal Membrane Oxygenation. *J ASAIO* 63:e52–e59.

### Impact Statement

- What is the key message of your article?
  - Cerebral blood flow and oxygenation are not well predicted by systemic proxies such as ECMO pump flow or blood pressure.
  - Continuous, quantitative, bedside monitoring of cerebral blood flow and oxygenation with optical tools enables new insight into the adequacy of cerebral perfusion during ECMO.
- What does it add to the existing literature?
  - A demonstration of hybrid diffuse optical and correlation spectroscopies to continuously measure cerebral blood oxygen saturation and flow in patients on ECMO, enabling assessment of cerebral autoregulation.
  - An observation of poor correlation of cerebral blood flow and oxygenation with systemic mean arterial pressure and ECMO pump flow, suggesting that clinical decision making guided by target values for these surrogates may not be neuroprotective.
- What is the impact?
  - ~50% of ECMO survivors have long-term neurological deficiencies; continuous monitoring of brain health throughout therapy may reduce these tragically common sequelae through brain-focused adjustment of ECMO parameters

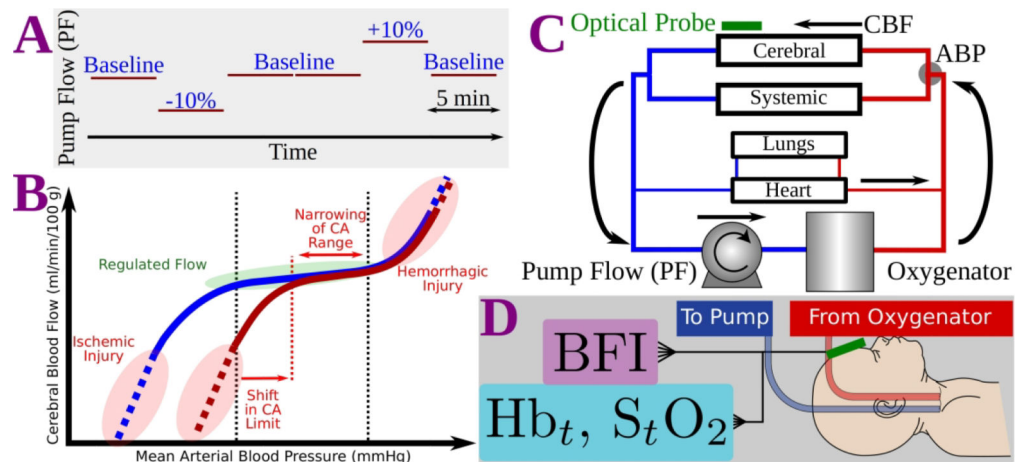


**Figure 1:**

(a) Timeline of dynamic measurement, showing nominal steps in ECMO pump flow. The actual change, number of steps, and rate of change was limited by the clinical team based on individual patient response. (b) Schematic of  $CBF$  vs.  $MAP(16)$ : at high and low  $MAP$ , flow is pressure-controlled. At blood pressures within the pressure limits of autoregulation (dotted lines), flow is regulated; outside this zone, the brain is at risk for hemorrhage or ischemia. The pressure limits of autoregulation are not well understood in neonates and are expected to change with disease state. For example, the lower limit may shift, narrowing the range of regulated flow (maroon curve). Schematics of: (c) blood circulation; and (d) FD-DOS/DCS monitoring during ECMO. Optical measurements include the DCS index of  $CBF$  ( $BFI$ ); and FD-DOS measurement of cerebral oxygen saturation ( $S_tO_2$ ) and total hemoglobin concentration ( $Hb_t$ ).

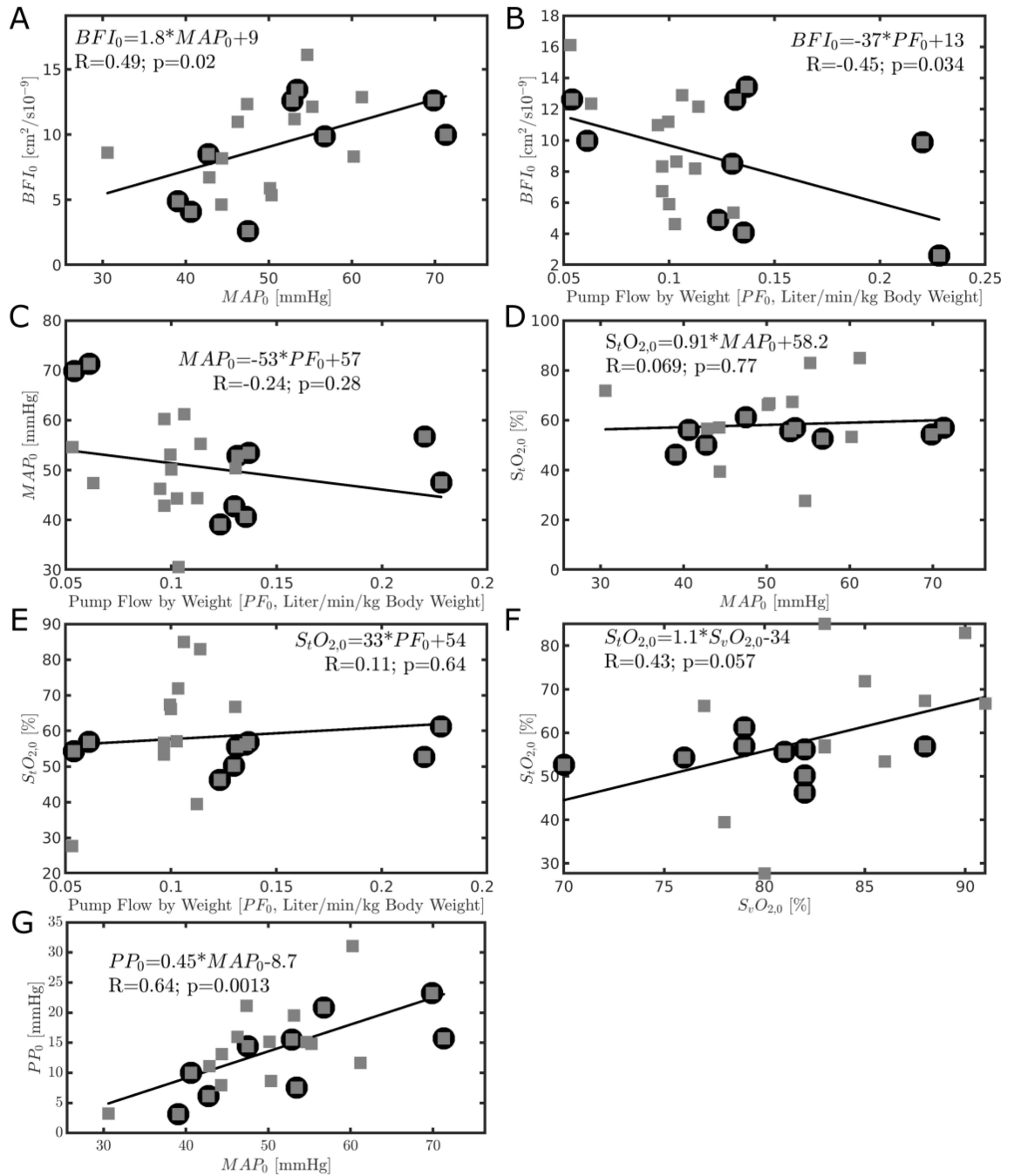


**Figure 2:** Comparison of cerebral and systemic parameters at clinically established (baseline) ECMO settings, in all subjects/days. DCS-measured Blood Flow Index (*BFI*) vs. (a) Mean Arterial Blood Pressure (*MAP*) and (b) pump flow (*PF*, normalized by patient weight). (c) *MAP* is not well correlated to pump flow. Cerebral oxygenation (*StO<sub>2</sub>*) is poorly correlated to *PF* (d) and *MAP* (e); it is trending to a weak correlation with venous oxygen saturation (*SvO<sub>2</sub>*) (f). Pulse pressure (*PP<sub>0</sub>*) was correlated with *MAP* (g). Black circles designate subjects who expired on ECMO. Lines represent a linear best fit; R is Spearman’s correlation coefficient.

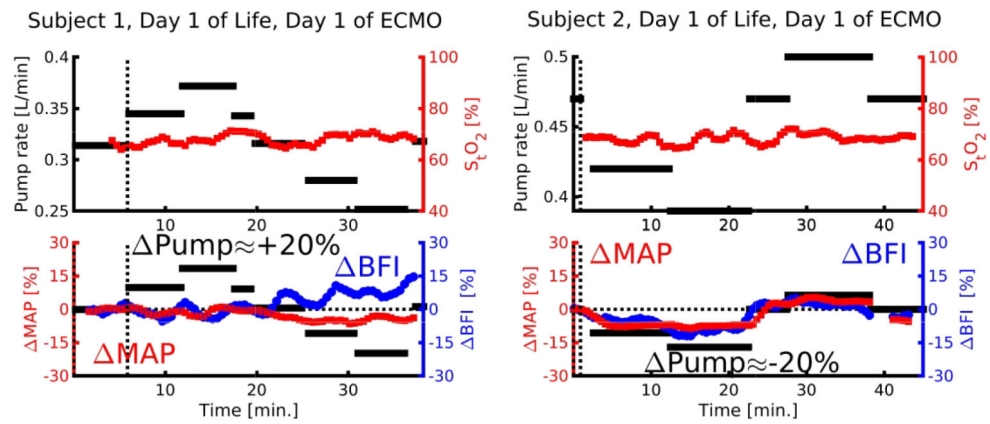


**Figure 3:**

Time courses of tissue oxygen saturation, and changes in *MAP* and *BFI* during *PF* manipulation over time for two exemplar subjects (#1, 2). *DCS<sub>x</sub>* (95% CI) for the monitoring sessions depicted here were  $-0.42$  (0.52,  $-0.31$ ) and  $0.71$  (0.65, 0.77). Fractional change in *PF*, *MAP*, and *BFI* are all plotted relative to baseline (between zero and vertical dotted line).

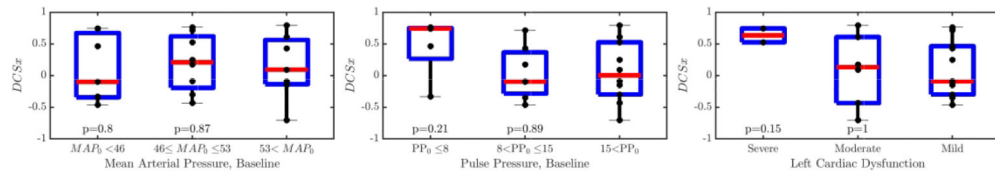


**Figure 4:**

All panels display data obtained across multiple days in 9 neonates on ECMO. *CA*, as measured by *DCSx*, is not predicted by (A) Mean arterial pressure ( $MAP_0$ , grouped by terciles), pulse pressure ( $PP_0$ ), or left cardiac dysfunction at baseline (Wilcoxon rank-sum).

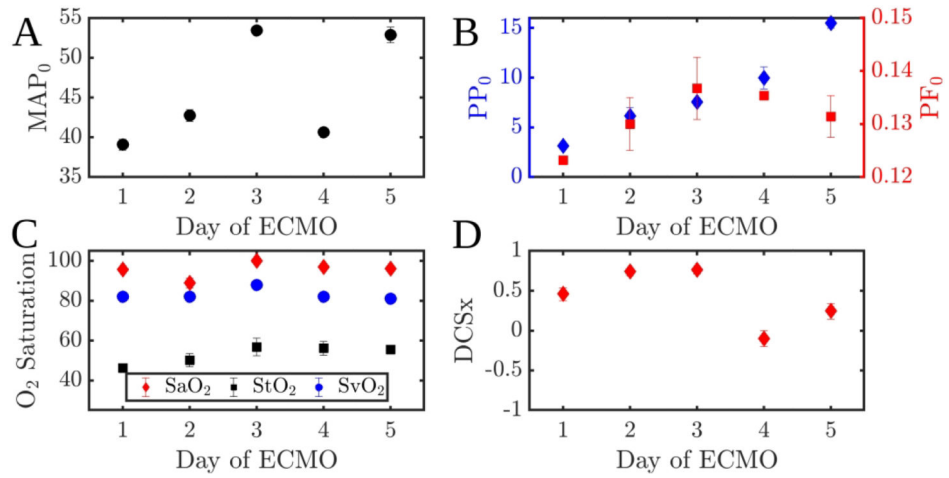


**Figure 5:** Longitudinal baseline measurements of  $MAP_o$  (A);  $PP_o$  and  $PF_o$  (B);  $StO_{2o}$ ,  $SvO_{2o}$ , and  $SaO_{2o}$  (C); and the optical  $DCSx$  CA index (D) for patient #7, who survived ECMO. Error bars denote standard deviation (A, B, C) and the 95% CI (D). On days 1, 2, and 4, the  $MAP_o$ ,  $SaO_{2o}$ , and  $SvO_{2o}$  changed little, however  $DCSx$  changed significantly.

**Table 1:**

Summary of patient demographic and diagnostic information.

#	Sex	Day of Life	Indication	# Meas.	ECMO duration (days)	Died on ECMO	Post ECMO Imaging	Post ECMO neuroimaging diagnosis
1	M	1	Pul. HTN	2	20	N	MRI	Subtle periventricular WM gliosis, old WMI
2	M	1	CDH	3	29	Y	NA	NA
3	M	2	Gastro.	2	20	N	MRI	Mild to moderate WMI
4	M	6	TOF	2	5	Y	NA	NA
5	M	1	CDH	4	26	Y	NA	NA
6	F	3	CDH	1	24	N	MRI	Mild microhemorrhages
7	F	1	Bivent Dys.	5	5	N	None	Head CT on ECMO showed left MCA stroke.
8	F	4	TOF, Pul. HTN	2	2	N	CT	Multiple microhemorrhages
9	M	1	CDH	1	1	N	MRI	None

Pul. HTN: Pulmonary Hypertension; CDH: Congenital Diaphragmatic Hernia; TOF: Tetralogy of Fallot; Bivent. Dys.: Biventricular dysfunction; WMI: Ischemic White Matter Injury; Gastro: Gastroschisis; # Meas.: Number of optical measurements; Day of Life & Weight: Age & weight at initiation of ECMO therapy. NA: Not applicable.

**Table 2.**

Summary statistics for baseline hemodynamic measurements and DCSx (Section 3.1)

Parameter	Overall ( $m=22$ )	Study day 1 ( $m=9$ )	Study day 2 ( $m=7$ )	Study day 3+ ( $m=6$ )	CV ( $n=7$ )
$PF_o$ (L/kg/min)	0.11 (0.10, 0.13)	0.10 (0.09, 0.13)	0.10 (0.07, 0.13)	0.12 (0.11, 0.14)	0.07 (0.03, 0.10)
$MAP_o$ (mmHg)	50 (44, 55)	47.5 (43, 53.5)	55.3 (44, 59.4)	51.5 (44.4, 53.4)	0.10 (0.08, 0.12)
$PP_o$ (mmHg)	14.6 (8.7, 16)	14.4 (6.78, 15.8)	20.9 (12, 22.7)	12.4 (9.98, 15.2)	0.26 (0.26, 0.31)
$SaO_{2o}$ (%)	97 (95, 99)	96 (95, 99)	98 (91, 100)	97 (96, 98)	0.02 (0.01, 0.04)
$SvO_{2o}$ (%)	82 (78, 85)	82 (79, 86)	82 (73, 85)	82 (78, 83)	0.04 (0.03, 0.07)
$StO_{2o}$ (%)	57 (53, 67)	59 (52, 67)	54 (53, 57)	57 (56, 66)	0.12 (0.09, 0.16)
$Hbt_o$ ( $\mu$ M)	47 (39, 54)	49.7 (40, 55.8)	42.7 (34, 45.5)	50.2 (41.5, 66.3)	0.12 (0.07, 0.19)
$BFI_o$ ( $\text{cm}^2/\text{s} \times 10^{-9}$ )	9.3 (5.9, 12.3)	8.63 (4.84, 11)	9.87 (8.36, 12.3)	10.4 (5.9, 12.9)	0.23 (0.19, 0.47)
$\mu'_{s,o}$ (785 nm) 1/cm	3.8 (3.2, 4.8)	4.61 (3.83, 4.85)	3.63 (3.17, 5.39)	3.63 (2.93, 3.82)	0.26 (0.18, 0.35)
$\mu_{a,o}$ (785 nm) 1/cm	0.11 (0.09, 0.12)	0.11(0.10, 0.12)	0.10 (0.09, 0.10)	0.11 (0.10, 0.14)	0.09 (0.04, 0.22)
$DCSx$	0.13 (-0.30, 0.61)	0.17 (-0.20, 0.57)	0.43 (-0.37, 0.71)	-0.10 (-0.30, 0.25)	0.86 (-0.32, 1.14)

All measurements were taken at baseline, e.g.,  $XQ$ .  $PF$ : pump flow,  $MAP$ : mean arterial pressure,  $PP$ : pulse pressure,  $SaO_2$ ,  $SvO_2$ : arterial/venous oxygen saturation,  $StO_2$ : tissue hemoglobin oxygen saturation,  $Hbt$ : tissue hemoglobin concentration,  $\mu_s'$ : reduced scattering coefficient,  $\mu_a$ : absorption coefficient, CV: Coefficient of Variation. All data: median (IQR). Coefficient of variation (standard deviation over mean) was calculated for each subject individually before median and IQR were calculated. No correction was made for multiple measurement days on some subjects (columns 2–5). Number of measurements: m; number of subjects: n. For 2 subjects with only a single monitoring session, the coefficient of variation could not be calculated. The coefficient of variation in  $DCSx$  was over three times larger than that of any other parameter.